Journal of Applied Fluid Mechanics, Vol. 11, No. 1, pp. 271-284, 2018.
Available online at www.jafmonline.net, ISSN 1735-3572, EISSN 1735-3645.
DOI: 10.29252/jafm.11.01.28167

Natural Convection in an Enclosure with a Discretely Heated Sidewall: Heatlines and Flow Visualization

M. Saglam[1], B. Sarper[2] and O. Aydin[1†]

[1] *Karadeniz Technical University Department of Mechanical Engineering, 61080 Trabzon, Turkey*
[2] *Gumushane University Department of Mechanical Engineering, 29100 Gumushane, Turkey*

†*Corresponding Author Email: oaydin@ktu.edu.tr*

(Received July 7, 2017; accepted September 12, 2017)

ABSTRACT

Natural convection inside a rectangular enclosure is investigated experimentally and numerically. One of the sidewalls is heated discretely by two flush-mounted heat sources. The other sidewall is kept at a constant temperature, while the horizontal walls are unheated. Heat dissipation rates of the heat sources are equal to each other. The aspect ratio of the enclosure (AR) is 2 and the working fluid is air (Pr=0.71). The study is focused on the validation of the two and three dimensional computations under real test conditions against experiments for various modified Rayleigh number values. Experimental study is performed for various modified Rayleigh numbers in the range of $7.7x10^5$ and $3.1x10^6$ while numerical part covers the values between 10^4 and $5x10^6$. Temperature measurements and flow visualization studies are performed in the experimental work, and streamlines, isotherms and heatlines are presented in the numerical part of the study. From the experimental and numerical studies, it is shown that two dimensional computations reflects the general characteristics of the problem, conduction and radiation heat transfer are not negligible, surface temperatures increase with the modified Rayleigh number and heatline approach is an important tool to analyze convective heat transfer.

Keywords: Natural convection; Electronics cooling; Rectangular enclosure; Discrete heating; Surface radiation; Conjugate; Flow visualization; Heatlines.

NOMENCLATURE

A	area
AR	aspect ratio of the enclosure
c_p	specific heat
D	enclosure depth
E	surface emissive power
F	body force
H	enclosure height
$\boldsymbol{H}$	heat function
$\boldsymbol{H}^*$	dimensionless heat function
h	surface heat transfer coefficient
I	current
k	thermal conductivity
L	enclosure length
Nu	Nusselt number
P	dimensionless pressure, Power
p	pressure
Pr	Prandtl number
R	resistance of the thin-film heaters
Ra^*	Modified Rayleigh number
s	width of the unheated sections
T	temperature
t	thickness
U, V	dimensionless velocity components
u, v	velocity components
Q	heat transfer rate
$\dot{q}$	heat generation
q''	durface heat flux
w	width of the heat sources
X,Y,Z	dimensionless cartesian coordinates
x,y,z	cartesian coordinates
α	thermal diffusivity
β	thermal expansion coefficient
ε	surface emissivity
θ	dimensionless temperature
ϑ	kinematic viscosity
ρ	density
Ψ	dimensionless stream function
ψ	stream function

Subscripts

c	cold surface
$cond$	conductive
$conv$	convective
cu	copper
ins	insulation material
k, j	surfaces in the radiation calculations
l	left

m	mean	*rad*	radiative
p	plexiglas	*s*	heat source

1. INTRODUCTION

Natural convection in enclosures has received a considerable research attention as it is encountered in many engineering applications including electronics cooling, building design, solar energy systems and nuclear energy.

Natural convection is a preferred heat transfer mechanism for cooling of electronic equipments because of its simplicity, absence of noise, freedom from electromagnetic interference, low maintenance cost and reliability in use. It requires no extra equipment such as pumps, valves and pipes and offers reliable, efficient and cheap cooling.

Majority of the studies in the existing literature have considered natural convection in enclosures due to either a horizontally or vertically imposed temperature difference. However, many of the systems or equipments in practice cannot be represented with this problem geometry. For example, electronic components are usually encountered as embedded in flat surfaces. Therefore, local or discrete heating cases should be studied for better representation of real situations.

Flack and Turner (1980) conducted an experimental study on natural convection in a rectangular enclosure with a discrete heat source which simulates high-power integrated circuits. They studied the effects of the aspect ratio, heater size and location. They developed heat transfer correlations for the studied problem and obtained optimal heater location and aspect ratio. Valencia and Frederick (1989) studied the problem of natural convection in a square enclosure with thermally half active and half inactive sidewalls numerically for various Rayleigh numbers and source-sink positions to obtain optimum positions for heat transfer. Chadwick *et al*. (1991) investigated natural convection in a rectangular enclosure with a single and a pair of localized flush-mounted heaters numerically and experimentally. They used Mach-Zehnder interferometry to visualize the temperature field and determine the heat transfer, and reported that the heat transfer was maximum when locations of the heaters are closer to the bottom of the enclosure for both single and pair heater configurations. Ahmed and Yovanovich (1991) carried out a numerical study on the effect of discrete isoflux or isothermal heater on natural convection in a square enclosure. They performed the study in a broad range of Rayleigh number values ($0 \leq Ra < 10^{10}$), lengths and positions of the heater. They reported that the relative heater size had a negligible effect on heat transfer when $Ra > 10^8$. Ho and Chang (1994) studied the effect of the aspect ratio of a rectangular enclosure on natural convection from four discrete heat sources numerically and experimentally. They developed correlations including modified Rayleigh number and enclosure aspect ratio to obtain the average Nusselt number and maximum temperature on each heat source surface. Heindel *et al*. (1995a) performed a validation study in an enclosure with a 3x3 heat source array using water and FC-77 as the working fluids for a conjugate natural convection problem. They studied the same geometry for two and three dimensional computational domains and compared the results against same experimental works, and reported that the two dimensional solutions reflect the general characteristics of the problem. Heindel *et al*. (1995b) studied the same problem numerically for different working parameters such as heater/fluid thermal conductivity ratios and different Rayleigh numbers. They reported that thermal spreading in the substrate increased with decreasing values of the Rayleigh number and increasing values of substrate/fluid thermal conductivity ratio, and thermal spreading in the substrate affects the circulation inside the cavity and maximum surface temperatures considerably. Hsu *et al*. (1997) carried out a numerical study on natural convection of micropolar fluids in a tilted enclosure heated by discrete heat sources from one of its walls. The effects of Rayleigh number, material properties of the fluid and tilting angle on heat transfer were investigated. They showed that microstructure had significant effects on convective heat transfer, and the average Nusselt number was lower for a micropolar fluid than that of the Newtonian fluid. Ramos *et al*. (1998) studied natural convection from two discrete heat sources placed on a sidewall of a rectangular enclosure numerically and experimentally by taking heat dissipation ratio, clearance between the heat sources and enclosure aspect ratio as working parameters. They concluded that the higher dissipation heat source must be positioned near to the ceiling of the enclosure. Tou *et al*. (1999) performed a numerical study on natural convection in a rectangular enclosure with a 3x3 array of flush mounted discrete heat sources for various liquids, enclosure aspect ratios and modified Rayleigh numbers. They pointed out that the heat transfer from the discrete heaters was non-uniform and maximum heat transfer occurred on the heaters positioned at the leading edge. Aydin and Yang (2000a, 2000b) investigated natural and mixed convection in enclosures with localized heating from below numerically. They obtained that the heat transfer increased with an increase in heat source thickness. Tou and Zhang (2003) studied the effects of inclination of the rectangular enclosure with a 3x3 heat source array numerically. Da Silva (2004) determined the optimum heat source placement via constructal theory in a naturally cooled square enclosure and reported that the heat sources must be positioned closer near to the leading edge and spacing between the heat sources must increase towards the ceiling. Aydin and Pop (2005) carried out a numerical study on natural convection from a discrete heater in a micropolar fluid filled enclosure. They focused on the effects of the

material parameter on momentum and heat transfer, and reported that an increase in material parameter decreased heat transfer. Calcagni *et al*. (2005) investigated the effects of heat source length on natural convection inside a square enclosure with localized heating from below and cooling from lateral walls for different Rayleigh numbers and heat source lengths numerically and experimentally. They obtained that an increase in the heat source length increased heat transfer. Corvaro and Paroncini (2007) investigated the effects of the localized heat source position on natural convection in a square enclosure by using holographic interferometry and 2D-PIV techniques experimentally, and numerically. Three different positions of the heat source were investigated, and evaluated that the symmetrical configuration was the best in terms of heat transfer. Bairi, and Bairi *et al*. (2008a, 2008b) conducted numerical and experimental studies to investigate the inclination effects on natural convection in an adiabatic enclosure heated discretely by three discrete heat sources and proposed Nu-Ra correlations to the engineers. Deng (2008) investigated natural convection inside a square enclosure with two and three discrete heat source-sink pairs on the enclosure walls numerically. It was shown that that the staggered arrangement of the source-sink pairs increased eddies in the enclosure and enhanced heat transfer. Corcione and Habib (2010) conducted a numerical study in an inclined square enclosure discretely heated from one side. They performed simulations for different sizes and locations of the heater, Rayleigh and Prandtl numbers, and inclination angles. They reported that the heat transfer got better for the intermediate positions of the heater and decreased when the heater was positioned on the top or bottom of the enclosure. They also pointed out that heat transfer increased with the Rayleigh and Prandtl numbers, and positive inclination angles. Kuznetsov and Sheremet (2011) carried out a numerical study on conjugate natural convection in an enclosure with a heat generating body on one of the sidewalls. Nardini and Paroncini (2012) numerically and experimentally studied natural convection inside a square enclosure with heat source-sink pairs on the sidewalls. They investigated the arrangement and size of the source-sink pairs on flow, measured the air temperature and heat transfer by holographic interferometry, and compared with numerical results. Ayachi *et al*. (2012) numerically investigated natural convection and surface radiation in a square enclosure with localized heat source-sink pairs by using heatline visualization for different heating modes, source-sink lengths and Rayleigh number values. It was shown that the emissivity value of the thermally active surfaces was important in terms of surface radiation while emissivity value of the thermally inactive surfaces was unimportant for the radiation heat exchange. Habib *et al*. (2014) performed an experimental study to obtain the effects of uniform or non-uniform heat source distribution on natural convection characteristics in an enclosure with three discrete heat source on its sidewall for turbulent flow conditions. They performed the study for three heating values and three different heat source locations for each case, and obtained that non-uniform arrangement of the heat sources improved the heat transfer. Mahapatra *et al*. (2015a) performed a parametric numerical study to obtain the active wall location for better heat transfer in a rectangular enclosure for three different values of aspect ratio and six different locations of the source-sink pair. They pointed out that the bottom-top configuration was good for temperature uniformity. Mahapatra *et al*. (2015b, 2016) numerically investigated natural convection inside an enclosure with two alternately active heat sources on the bottom of the enclosure for different switch time periods and Rayleigh numbers. They reported that the heat transfer increased with an increase in pulsation frequency and heat transfer was higher than the steady state case. Purusothaman *et al*. (2016a, 2016b) performed numerical studies on natural convection in a nanofluid filled enclosure with a 3x3 discrete heat source array. They focused on the effects of different nanofluids, nanoparticle volume fraction, enclosure aspect ratio with different boundary conditions on heat transfer characteristics at various Rayleigh number values. Naffouti *et al*. (2016) conducted a study to optimize heat transfer in a two dimensional enclosure heated from the bottom with two identical heated blocks and cooled from the sides. They performed numerical simulations for various Rayleigh numbers, spacings between the blocks, block heights and enclosure aspect ratios. They reported that the most important parameters on hydrodynamic and thermal fields were the block height and enclosure aspect ratio. The authors also pointed out that increasing the spacing between the blocks and Rayleigh number increase heat transfer. Nardini *et al*. (2016) conducted an experimental and numerical study to analyze the effects of the position of a heat source on the bottom of the enclosure with two sink pairs on each of the lateral walls. They performed the study for various Rayleigh number values and three different heat source positions and obtained the optimum position of the source to enhance heat transfer. Karatas and Derbentli (2017) performed an experimental study to investigate the effects of enclosure aspect ratio in a rectangular enclosure with a localized heat source. Only one wall of enclosure containing localized heat source was thermally active and other walls of the enclosure was thermally inactive and insulated. They developed correlations for the Nusselt number including the quantities of Rayleigh number and enclosure aspect ratio, and also measured temperatures inside the flow domain.

As it is seen in the literature review, although there are numerous studies on natural convection in enclosures, studies using flow visualization techniques and heatlines approach are limited. In order to better understand the flow and heat transfer mechanism, these techniques have been used together in the study. It should also be noted many of the studies in the existing literature are numerical while experimental studies are scarce. The main objective of this study is to examine the heat

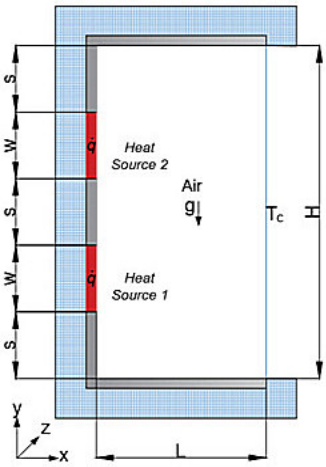

(a)

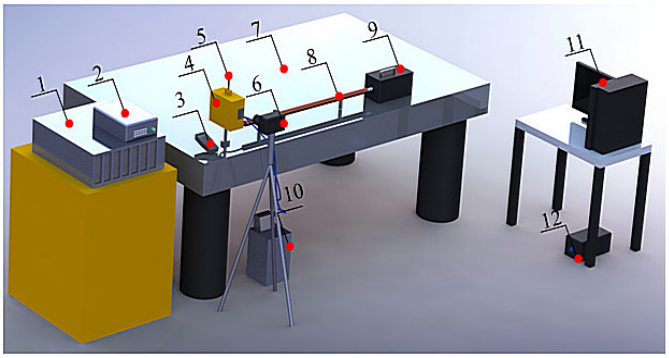

1. DC Power Supply
2. Data Acquisition System
3. Hand Type Data Logger
4. Test Cell
5. Diode Laser
6. CCD Camera
7. Optical Table
8. Copper Pipe
9. Fog Generator
10. Thermostatic Bath
11. Computer
12. UPS

(b)

Fig. 1. (a) Schematic of the problem, (b) Experimental Set-up.

transfer in rectangular enclosure with a pair of discrete heat source on its sidewall which simulates an electronic package and to validate the two and three dimensional computations under realistic conditions. The effects of the modified Rayleigh number on fluid flow and heat transfer are investigated both experimentally and numerically.

2. EXPERIMENTAL APPARATUS AND PROCEDURE

The schematic of the problem under investigation and experimental set-up is shown in Fig. 1. Experiments are carried out in a discretely heated rectangular enclosure. One of the sidewalls includes two discrete heat sources and unheated parts. The other sidewall is maintained at a constant temperature, while the horizontal walls are unheated. The enclosure was machined as 63.5 mm height (H), 31.75 mm length (L) and 152.4 mm depth (D). The discretely heated sidewall is divided into five equal parts. The discretely heated sidewall and horizontal walls are made of 10 mm-thick plexiglas due to its transparency and low thermal conductivity (k_p=*0.19 W/mK*). The heat source surfaces are made of copper (k_{cu}=*387.6 W/mK*) with 1.5 mm thickness, 12.7 mm width and 152.4 mm depth. 12.7 mm wide thin-film flexible heaters are used at the back of the copper surfaces. The right vertical wall of the enclosure is considered as the cold-isothermal wall made of 1.5 mm thick copper, which is cooled by a thermostatic bath. Because of its high thermal conductivity and low thermal capacity, copper is used on the thermally active surfaces. All of the copper surfaces are polished to minimize radiation heat transfer. The test cell is insulated with 60 mm thick XPS foam board (k_{ins}=*0.035 W/mK*) to minimize heat losses to the environment.

Temperature measurements are performed at the mid-plane ($D/2$) of the plexiglass walls and copper plates with twenty two 0.4 mm-diameter T-type thermocouples. The thermocouples are placed 1 mm under each of the plexiglass walls and copper surfaces. Apart from the enclosure walls and copper surfaces, 2 thermocouples are placed at the inlet and outlet ports of the water jacket in order to control the water temperature (see Fig.2). The test cell is placed on an optical table to minimize the vibration effects and oriented by using a digital protractor.

At the beginning of each experiment, temperature was kept at 24˚C by an air-conditioner. Temperature of the cold wall is maintained at 24˚C

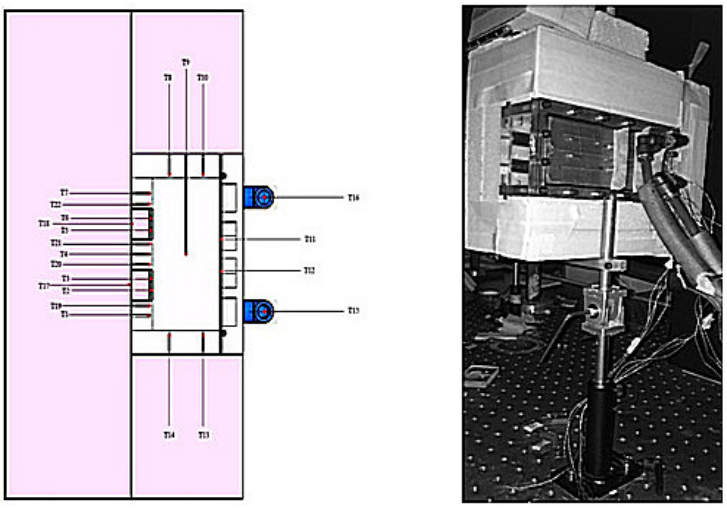

(a) (b)

Fig. 2. (a) Thermocouple settlements at the mid-plane of the enclosure (D/2), (b) Test section.

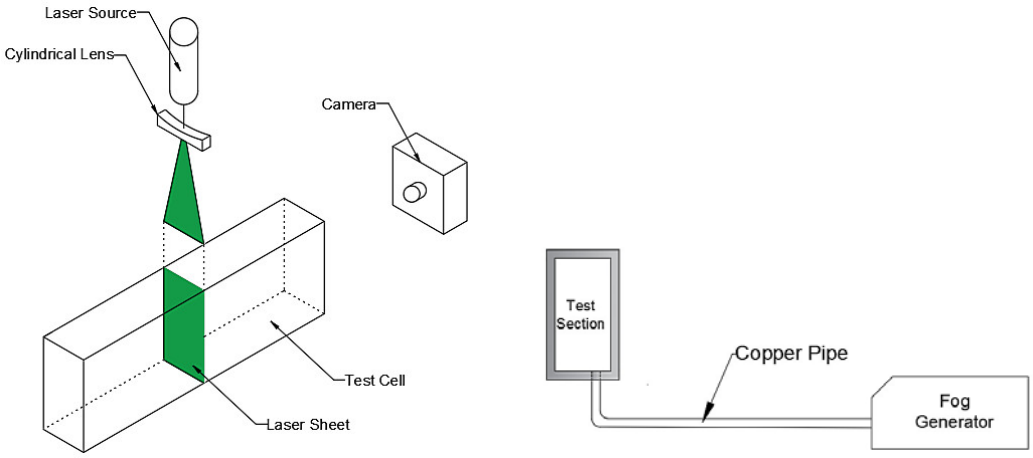

(a) (b)

Fig. 3 Flow visualization unit

with a thermostatic bath. For each experiment, the flow is considered to have reached steady-state when temperature measurements do not change with time anymore.

Smoke visualization technique is applied to display flow field. Safex F2010 fog generator, a 50 mW diode laser and a camera were used to visualize the flow domain. After temperatures have reached steady state, flow visualization process is started. The smoke is injected to the enclosure by being passed into a long copper pipe to reduce its temperature. Temperature of the smoke is measured with a thermocouple at the outlet of the copper pipe and it is observed that, smoke is entered into the test section at a temperature close to that of the cold wall. The sketch of the flow visualization unit is represented in Fig. 3.

The required power input to the flexible heaters is calculated by Eq. (1) and supplied by a modular DC power supply system (Agilent 66000A with 66102A power modules).

$$P = I^2 R = q_m^{"} A_s \tag{1}$$

$$I = \sqrt{\frac{q_m^{"} A_s}{R}} \tag{2}$$

where P, I and R denote the power input, current and resistance of the heaters, respectively. $q_m^{"}$ is the heat flux from the thin-film flexible heaters to the copper plates and A_s is the surface area of the copper plates in contact with the heaters.

3. NUMERICAL STUDY

In the numerical computations, continuity, momentum and energy equations are solved via ANSYS Fluent software. Flow is assumed to be steady and laminar. Fluid is assumed to be incompressible with constant properties except density. Boussinesq approximation is implemented to model the density change with temperature. Although thermal conductivity of the plexiglass is

low, experimental results show that conduction heat loss cannot be neglected. Therefore, conduction heat transfer inside the plexiglass walls, copper plates and insulation material is taken into account in the numerical analysis. Detailed comparisons are given between obtained experimental and numerical results.

3.1 Governing Equations and Boundary Conditions

For a three-dimensional, laminar and incompressible flow, the conservation equations for mass, momentum and energy equations are given as follows:

$$\frac{\partial u}{\partial x}+\frac{\partial v}{\partial y}+\frac{\partial w}{\partial z}=0 \tag{3}$$

$$u\frac{\partial u}{\partial x}+v\frac{\partial u}{\partial y}+w\frac{\partial u}{\partial z}= -\frac{1}{\rho}\frac{\partial p}{\partial x}+\vartheta\left(\frac{\partial^2 u}{\partial x^2}+\frac{\partial^2 u}{\partial y^2}+\frac{\partial^2 u}{\partial z^2}\right) \tag{4}$$

$$u\frac{\partial v}{\partial x}+v\frac{\partial v}{\partial y}+w\frac{\partial v}{\partial z}=-\frac{1}{\rho}\frac{\partial p}{\partial y} +\vartheta\left(\frac{\partial^2 v}{\partial x^2}+\frac{\partial^2 v}{\partial y^2}+\frac{\partial^2 v}{\partial z^2}\right)+F \tag{5}$$

$$u\frac{\partial w}{\partial x}+v\frac{\partial w}{\partial y}+w\frac{\partial w}{\partial z}= -\frac{1}{\rho}\frac{\partial p}{\partial z}+\vartheta\left(\frac{\partial^2 w}{\partial x^2}+\frac{\partial^2 w}{\partial y^2}+\frac{\partial^2 w}{\partial z^2}\right) \tag{6}$$

$$u\frac{\partial T}{\partial x}+v\frac{\partial T}{\partial y}+w\frac{\partial T}{\partial z}=\alpha\left(\frac{\partial^2 T}{\partial x^2}+\frac{\partial^2 T}{\partial y^2}+\frac{\partial^2 T}{\partial z^2}\right) \tag{7}$$

where u, v and w are the velocity components in the x, y and z directions. g is the gravitational acceleration. ϑ is the kinematic viscosity, and α is the thermal diffusivity of the fluid. Body force is defined as:

$$F=\beta g(T-T_0) \tag{8}$$

β denotes the thermal expansion coefficient of the fluid.

In the solid region:

$$\frac{\partial^2 T}{\partial x^2}+\frac{\partial^2 T}{\partial y^2}+\frac{\partial^2 T}{\partial z^2}+\frac{\dot{q}}{k}=0 \tag{9}$$

The modified Rayleigh number is defined as:

$$Ra^*=\frac{g\beta \dot{q} L^4 t_h}{k\vartheta\alpha} \tag{10}$$

where $\dot{q}$ denotes the volumetric heat generation inside the heaters, t_h is the thickness of the heaters, and k is the thermal conductivity of the fluid.

Boundary conditions are as follows:

At x=0: u=v=w=0 and

$$-k_s\frac{\partial T}{\partial x}=-k_f\frac{\partial T}{\partial x}+q''_{rad,net} \tag{11}$$

At x=L: u=v=w=0 and T=T_c (12)

At y=0: u=v=w=0 and

$$-k_s\frac{\partial T}{\partial y}=-k_f\frac{\partial T}{\partial y}+q''_{rad,net} \tag{13}$$

At y=H: u=v=w=0 and

$$-k_s\frac{\partial T}{\partial y}=-k_f\frac{\partial T}{\partial y}+q''_{rad,net} \tag{14}$$

At z=*0*: u=v=w=0 and

$$-k_s\frac{\partial T}{\partial z}=-k_f\frac{\partial T}{\partial z}+q''_{rad,net} \tag{15}$$

At z=D: u=v=w=0 and

$$-k_s\frac{\partial T}{\partial z}=-k_f\frac{\partial T}{\partial z}+q''_{rad,net} \tag{16}$$

where s and f denote the solid and fluid, respectively. $q''_{rad,net}$ represents the net radiative heat flux from the boundary and it is correspond to the difference of the outgoing and incoming radiation heat fluxes.

Convection flux boundary condition with the heat transfer coefficient, h=7 W/m^2 is implemented at the outer surfaces of the insulation material.

$$q''=h(T-T_{amb}) \tag{17}$$

From the energy balance on the copper surfaces:

$$Q_{conv}=Q_{tot}-Q_{cond}-Q_{rad} \tag{18}$$

Here, Q_{tot} is the total heat input and it is equal to the P described in Eq. (1). Q_{conv} is the convection heat transfer rate, Q_{cond} is the conduction heat loss from the copper plate to the plexiglass and insulation material, and Q_{rad} is the radiation heat loss from the copper surfaces.

The local heat transfer coefficient on the copper surface is:

$$h=\frac{Q_{conv}}{A_s(T_s-T_c)} \tag{19}$$

Therefore, local and mean Nusselt numbers on the copper surfaces are calculated by the following equations:

$$Nu=\frac{hL}{k} \tag{20}$$

$$Nu_m=\frac{\bar{h}L}{k} \tag{21}$$

Governing equations along with the boundary conditions are solved using ANSYS Fluent software. Pressure-based solver is selected which is

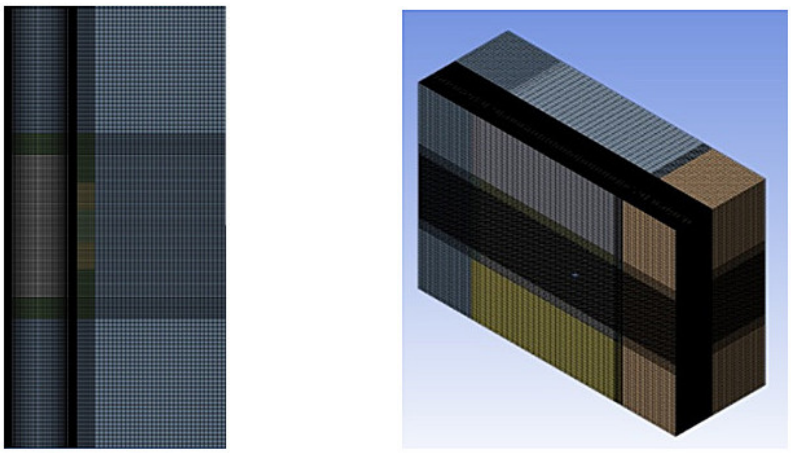

(a) (b)

Fig. 4. Mesh structure of the numerical models.

developed for low-speed incompressible flows. SIMPLE algorithm is used to solve pressure-velocity coupling. Discretization of the momentum and energy equations is provided by the second-order upwind scheme and pressure interpolation is carried out with PRESTO scheme.

3.2 Radiation Calculation

Radiation heat transfer between surfaces is taken into account by using surface to surface radiation method (S2S). In this method, all of the surfaces are considered as opaque, diffuse and gray. The working fluid, air is considered as a non-participating medium. Convergence criteria is taken as 10^{-6} for the radiation calculations. View factors are calculated by the program using face to face basis with ray tracing method (ANSYS Inc., 2013). The model equations are given as follows:

The incident energy flux to the surface k from all other surfaces is:

$$q''_{in,k} = \sum_{j=1}^{N} F_{kj} q''_{out,j} \tag{22}$$

Radiosity of the surface k is:

$$J_k = E_k + (1-\varepsilon_k) \sum_{j=1}^{N} F_{kj} J_j \tag{23}$$

where $j=1,2,3,...,N$

In Eq. (23), E_k denotes the emissive power of the surface k.

For the radiation calculations, emissivity values of the copper and plexiglass surfaces are taken as 0.05 and 0.85, respectively.

3.3 Grid Structure

Two and three-dimensional solution domains were created in order to compare heat source temperatures and streamlines between experiments and numerical studies. A non-uniform mesh structure is used in the numerical computations. It is seen from Fig.4, smaller mesh size is used near the boundaries where temperature and density changes are substantial. In order to calculate temperature gradients in the thermal boundary layer accurately, finer mesh structure is used in x and y directions while coarse mesh covers in z direction.

Mesh independence studies have been performed in order to make the numerical computations independent from the mesh structure for both 2D and 3D situations. Four different grid structures, namely, 51x51, 76x76, 101x101 and 126x126, and three different mesh sizes including 51x51x25, 76x76x25 and 101x101x25 have been checked for the two and three dimensional calculations at $Ra=2.3x10^6$, respectively. Results were obtained for the mean Nusselt numbers on the heat source surfaces and the mesh independence study showed that 101x101 grid structure provide numerical accuracy in two dimensional computations, and 101x101x25 grid structure was seen enough for three dimensional computations (See Table 1).

Table 1 Mesh independence study

2D Model				
	Heat Source 1 Nu_m	Heat Source 2 Nu_m	Change (%)	
51x51	7.56	5.29	-	-
76x76	7.52	5.25	0.614	0.862
101x101	7.50	5.23	0.233	0.343
126x126	7.49	5.22	0.120	0.197
3D Model				
76x76x25	7.59	5.32	-	-
101x101x25	7.61	5.35	0.280	0.459
126x126x25	7.61	5.34	0.125	0.194

3.4 Heatlines Approach

Heatlines approach was first presented by Kimura and Bejan (1983) to show energy transfer in flow field. They stated the definition of the heatlines as follows: "In convection problems, the energy transfer in flow field is sum of the heat diffusion and enthalpy. For such a flow field, an ***H***(x,y)

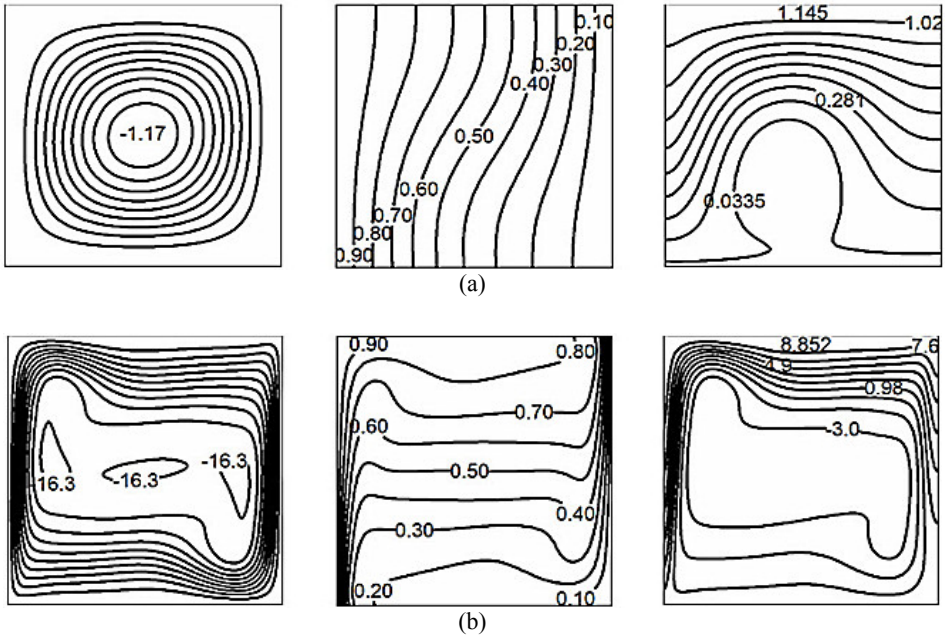

Fig. 5. Streamlines, isotherms and heatlines: (a) Ra*=10^3, (b) Ra*=10^6.

function could be defined where net energy transfer is zero through every constant ***H*** line".

Mathematically, heatlines could be expressed as below:

$$\frac{\partial \boldsymbol{H}}{\partial y} = \rho c_p u(T - T_0) - k\frac{\partial T}{\partial x}\,;\quad \frac{\partial \boldsymbol{H}}{\partial x} = \rho c_p v(T - T_0) - k\frac{\partial T}{\partial y} \tag{24,25}$$

where $\partial \boldsymbol{H}/\partial x$ and $\partial \boldsymbol{H}/\partial y$ denote the net energy flow except the surface radiation in x and y directions, respectively.

Subtracting these two equations side by side after taking first derivative, the equation below could be obtained.

$$\frac{\partial^2 \boldsymbol{H}}{\partial x^2} + \frac{\partial^2 \boldsymbol{H}}{\partial y^2} = \rho c_p \left[\frac{\partial (u(T - T_0))}{\partial y} - \frac{\partial (v(T - T_0))}{\partial x}\right] \tag{26}$$

where T_0 is the lowest temperature value in the flow field.

With the use of no-slip boundary condition at the wall-to-fluid interfaces, boundary conditions necessary for the solution of Eq. (26) are as follows:

$$\boldsymbol{H} = \boldsymbol{H}(L,0) + \oint_c k_f \frac{\partial T}{\partial n} \partial s \tag{27}$$

$\boldsymbol{H}(L,0)$ is taken as zero for the reference point. Although heatlines are presented in dimensional form in this study, it can be non-dimensionalized with the equation given below.

$$\boldsymbol{H}^* = \frac{\boldsymbol{H}}{\dot{q} t_h L} \tag{28}$$

In order to solve the Eq. (26), firstly, continuity, momentum and energy equations must be solved. Required data for the solution of the Eq. (26) are exported from ANSYS Fluent after the problem being solved. A Matlab code is generated to solve the Eq. (26). Successive substitution method is applied until relative error value is lower than 10^{-6}. The accuracy of numerical algorithm is validated against the results of Deng and Tang (2002).

Streamlines (□), isotherms (θ) and heatlines (***H****) obtained in the present study for validation are represented in Fig. 5. Figures plotted for non-dimensional form as follows:

$$\Psi = \frac{\psi}{\alpha}, \theta = \frac{T\text{-}T_c}{T_h\text{-}T_c}, \boldsymbol{H}^* = \frac{\boldsymbol{H}}{k_f (T_h\text{-}T_c)} \tag{29}$$

4. RESULTS AND DISCUSSION

Natural convection inside a rectangular enclosure heated by two flush-mounted discrete heat sources placed on its one side and cooled from the other side is investigated experimentally and numerically. Heat dissipation rates of the heat sources are the same. The aspect ratio of the enclosure (AR) is 2 and the working fluid is air. Experimental study covers four different modified Rayleigh number values (Ra*=7.7x10^5, 1.4x10^6, 2.3x10^6 and 3.1x10^6) while numerical part is in a wider range (Ra*=10^4-5x10^6). 2D and 3D investigations are carried out under laminar flow conditions.

Figure 6 shows the numerical and experimental streamlines obtained at mid-plane ($D/2$) of the enclosure for Ra*=7.7x10^5 and 3.1x10^6. For each case, fluid heated by discrete heat sources ascends through the left vertical wall, then faces the ceiling, descends along the cold wall and finally moves horizontally along the bottom. Along with the boundary conditions, main circulation inside the

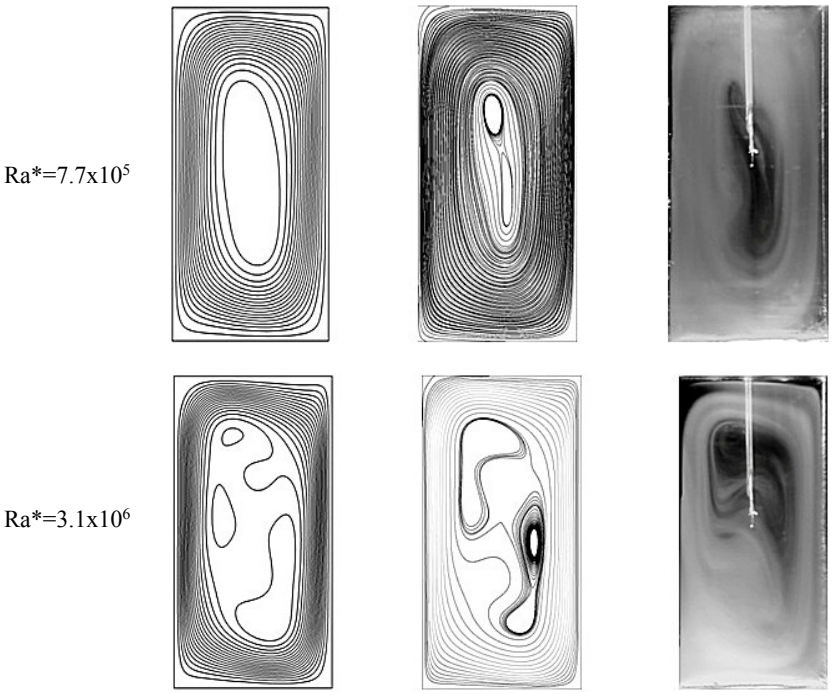

Fig. 6. Comparison of streamlines for Ra*=7.7x10^5 and Ra*=3.1x10^6 at the mid-plane of the enclosure (D/2): (a) 2D-numerical, (b) 3D-numerical, (c) experimental.

enclosure occurs in the clockwise direction. Single cell occupies the enclosure in 2D situation while secondary cell structure takes place in 3D and experimental cases at Ra*=7.7x10^5. Multicellular structure is seen for Ra*=3.1x10^6 for both cases. Secondary and tertiary cells cover center of the enclosure and boundary layer gets thinner depending on the circulation intensity. As it can be seen from the Fig. 6, although three-dimensional streamlines are more consistent with the experimental results, two-dimensional streamlines reflect the general characteristics of the flow satisfactorily.

Temperature distribution on the left sidewall and the heat source surfaces with the modified Rayleigh number is demonstrated in Fig 7. Temperature variation is represented for experimental measurements and numerical computations with or without surface radiation at the mid-plane of the enclosure (*D/2*). As it is seen from the Fig. 7, numerical and experimental surface temperatures are in a good agreement with each other and they follow the same trend. Surface temperatures increase towards the heat sources, get maximum value on the heat source surfaces and decrease again depending on the boundary conditions and conduction heat transfer inside the enclosure walls. Temperatures on the heat source surfaces are constant since thermal conductivity of the copper is high. Dimensions of the test section are specified to treat the flow is two-dimensional but, as seen from Fig. 7, heat losses to the third dimension are still exist. In addition, the effect of the surface radiation on temperature variation on the left sidewall is clearly seen. Surface temperatures obtained via 2D numerical computations with surface radiation are always higher than those of 3D numerical computations. This is because of the number of the radiating surfaces. When numerical computations with or without surface radiation are compared with each other, temperature values obtained via numerical models considering surface radiation are found to be lower than those not considering surface radiation. Temperature values obtained via 3D computations with surface radiation are found to be very close to those experimental. It is also shown that temperature values obtained via 2D computations with radiation are also within the acceptable limits and reflects the general characteristics.

The mean Nusselt number variation with modified Rayleigh number is seen in Fig. 8. As expected, mean Nusselt number values on the heat source surfaces increase with Ra*. As it can be seen from the figure, the mean Nusselt numbers obtained with two and three-dimensional computations are in a fairly good agreement with each other and maximum deviation between the results is %3. Therefore, two-dimensional model is found to be sufficient.

Streamlines, isotherms and heatlines are displayed in Fig. 9 for various values of the modified Rayleigh number at the mid-plane (*D/2*) of the enclosure. The results are presented in dimensional form. For the isotherms given, values are presented as the temperature difference (T-T_c) where T_c is the cold wall temperature. In the heatlines, results are presented for heat transfer rate per unit length [W/m]. At Ra*=10^4, viscous forces are dominant

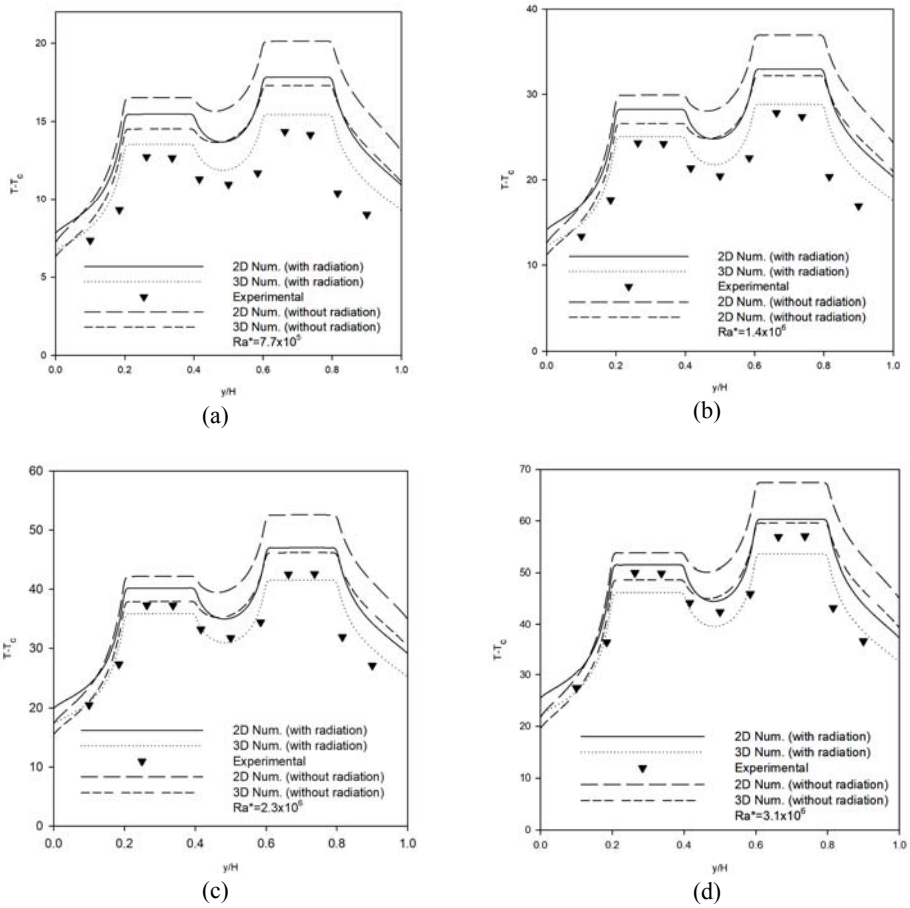

Fig. 7. Comparison of numerical and experimental surface temperatures on the left sidewall at the mid-plane of the enclosure (D/2).

over buoyancy forces, and the circulation inside the enclosure is so weak. Isotherms are parallel to the vertical walls, heatlines are almost perpendicular to the isotherms and this situation suggests that conduction regime is effective in the flow domain. With an increase in the modified Rayleigh number, circulation intensity increases, hydrodynamic boundary layer gets thinner and cores of the cells moves upward. Isotherms and heatlines slightly deviate, and convection heat transfer starts to become dominant over conduction.

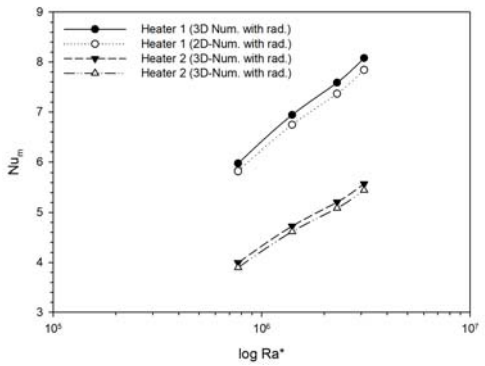

Fig. 8. Comparison of the mean Nusselt number values for 2D and 3D numerical computations at the mid-plane of the enclosure (D/2).

It is seen from the figure that, distortion of the isotherms and heatlines increases more, isotherms are more packed adjacent to the heat sources when the modified Rayleigh number gets values greater than 10^5. Especially at Ra*=10^6 and 5x10^6, isotherms are parallel to the unheated horizontal walls in the center of the enclosure, and thermal boundary layer is thinner near the thermally active walls, and heatlines are denser at these regions, which causes increased energy transport. When heatlines are examined, it is seen that convection heat transfer from the heat sources to the cold wall is concentrated at the upper region of the enclosure, and an inactive region occurs at the right bottom of the enclosure, especially at higher Ra* values. As a result of the presence of unheated regions on the left sidewall, conduction heat loss exists from the heat sources to the unheated regions as mentioned before in Fig. 7. This increases the temperature of the unheated regions, and convection heat transfer occurs from these regions to air. As it can be seen from Fig. 9, heatlines lie between the unheated parts of the left sidewall and the cold surface. Air in contact with heated surfaces rises and its temperature gradually increases. This results in heat transfer from air to the ceiling of the enclosure. In addition, as it can be seen from the heatlines, heat transfer from the base of the enclosure to the cold surface occurs as a result of conduction heat transfer.

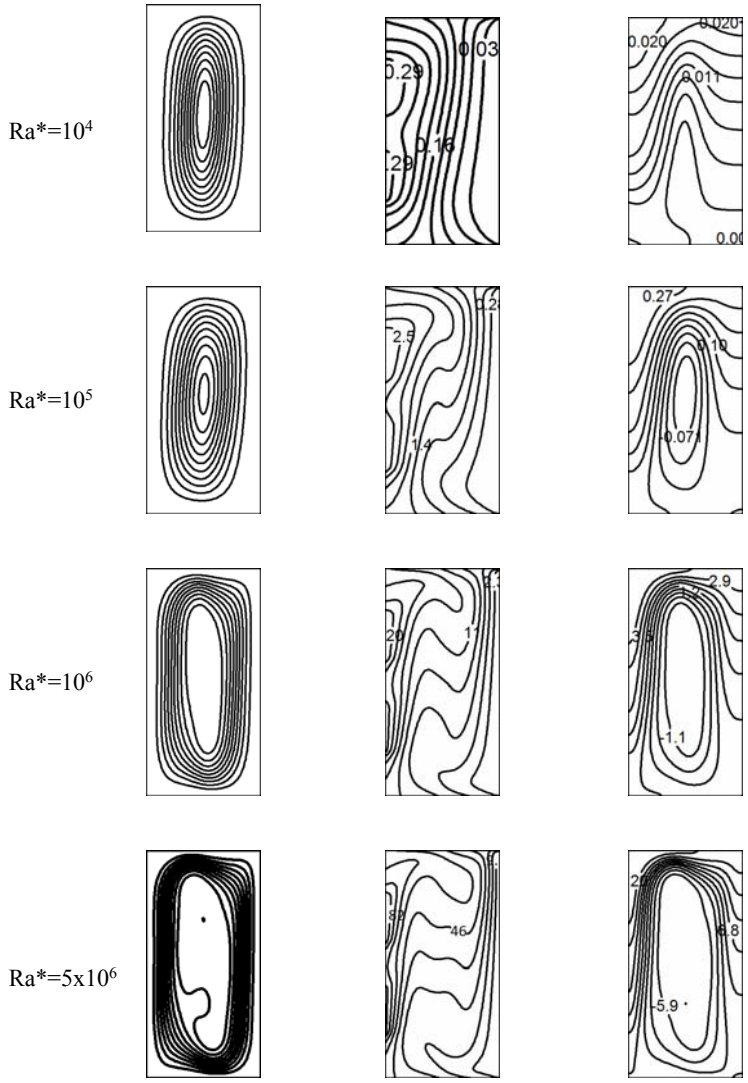

Fig. 9. Streamlines, isotherms and heatlines at different modified Rayleigh number values at the mid-plane of the enclosure (D/2).

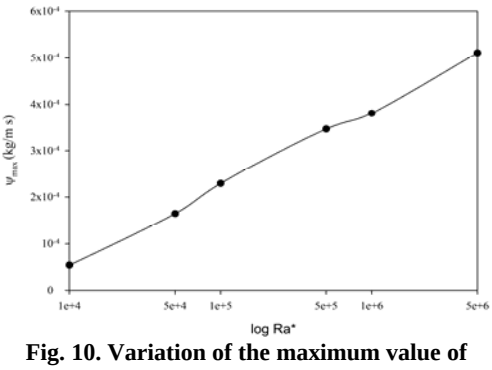

Fig. 10. Variation of the maximum value of stream function with modified Rayleigh number.

The effect of the modified Rayleigh number on maximum stream function value is demonstrated in Fig. 10. As it is clearly seen from the figure, flow is quiet weak for all of the working Ra* values. At lower Ra* values, viscous forces are dominant over buoyancy forces, and the fluid is almost stagnant. With increasing Ra*, viscous forces and buoyancy forces becomes balanced and circulation intensity inside the enclosure increases. A further increase in Ra* causes the advection terms to become dominant in the main flow and maximum value of the stream function increases.

Figure 11 shows the variation of the local Nusselt number on the heat source surfaces for various values of the modified Rayleigh number. The main circulation inside the enclosure is in the clockwise. Fluid in a contact with the heat sources ascends along the left vertical wall and descends throughout the cold isothermal wall. Colder fluid contacts with the lower heat source first and warms up. For this reason, heat transfer from the first heat source is more compared with the second heat source. As it is seen, local Nusselt number gets the maximum value at the leading edge of the heat sources then decreases along the heat source, takes the minimum

value and then increases again towards the trailing edge. The point of the minimum value of the local Nusselt number shifts up, and this becomes apparent with an increase in Ra*. At Ra*=10^4, local Nusselt number variation on the discrete heat sources has a symmetrical character. The local Nusselt number takes its maximum value at the leading edge of the heat source 1 while it is maximum at the trailing edge of the heat source 2. This situation occurs especially at lower values of Ra*, where conduction is the dominant heat transfer mechanism inside the enclosure and it disappears beyond Ra*=10^4. This can also be seen from the symmetrical structure of the isotherms within the thermal boundary layers at Ra*= 10^4 (See Fig. 9).

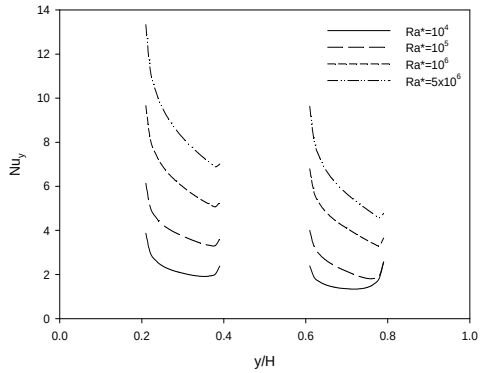

Fig. 11. Local Nusselt number variation on heat source surfaces at different modified Rayleigh number values at the mid-plane of the enclosure (D/2).

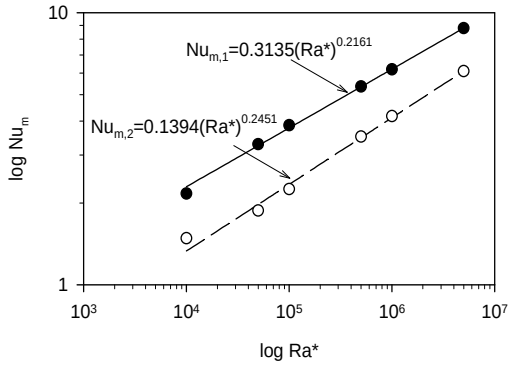

Fig. 12. The variation of the mean Nusselt number with modified Rayleigh number on heat source surfaces.

Effect of the modified Rayleigh number on mean Nusselt number is represented in Fig. 12. The figure shows that Ra* doesn't have a significant effect on Nu_m, and conduction is dominant at Ra*=10^4. Effect of the Ra* becomes important beyond Ra*=10^4, recirculation intensifies and convection heat transfer becomes apparent. As it is seen from the figure, correlation equations are obtained based on the numerical computations in the range of Ra*=10^4-5x10^6. The correlation equations for the first heat source and second heat source predict the numerical data with an average error of 1.62% and 3.79%, respectively.

Nu-Ra* correlations for the heat sources are given as follows:

$$Nu_{m,1} = 0.3135(Ra^*)^{0.2161} \text{ for heat source 1} \quad (30)$$

$$Nu_{m,2} = 0.1394(Ra^*)^{0.2451} \text{ for heat source 2} \quad (31)$$

5. CONCLUSION

In this study, natural convection inside a rectangular enclosure with a discretely heated sidewall has investigated experimentally and numerically. The following drawings can be drawn from the study:

- Both two and three dimensional simulations have been conducted. Comparison of the simulation results with the experimental ones showed that two-dimensional analysis was satisfactory.
- A conjugate heat transfer analysis has been conducted by including conduction in the enclosure walls. It is disclosed that conduction inside the sidewalls of the enclosure are too critical and it is considerable not to neglect.
- Surface radiation effects has been included in the analysis, which were shown to affect the heat transfer considerably.
- It is emphasized that heatlines approach is important to better understand the regarding heat transfer phsyics.
- Surface temperature of the left sidewall changes depending on the boundary conditions and modified Rayleigh number. Heat source temperatures remain nearly uniform due to the high conductivity of the heat source material, i.e. copper.
- Surface temperature of the first heat source is lower where the fluid in contact with the heat source is colder.
- As expected, circulation intensity and convective heat transfer increases as the modified Rayleigh number increases.

ACKNOWLEDGEMENTS

This study is supported by The Scientific and Technological Research Council of Turkey (TUBITAK) with project number of 114M589.

REFERENCES

ANSYS Inc. (2013), *ANSYS Fluent User's Guide Release 15*.

Aydin, O. and I. Pop (2005). Natural convection from a discrete heater in enclosures filled with a micropolar fluid. *International journal of engineering science 43*(19), 1409-1418.

Aydin, O. and W. J. Yang (2000). Natural convection in enclosures with localized heating from below and symmetrical cooling from

sides. *International Journal of Numerical Methods for Heat and Fluid Flow 10*(5), 518-529.

Aydin, O. and W. J. Yang (2000). Mixed convection in cavities with a locally heated lower wall and moving sidewalls. *Numerical Heat Transfer: Part A: Applications 37*(7), 695-710.

Baïri, A. (2008). Transient thermal characteristics of airborne electronic equipment with discrete hot bands in square cavities. *Applied Energy 85*(10), 951-967.

Baïri, A., J. G. de María, N. Laraqi and N. Alilat (2008). Free convection generated in an enclosure by alternate heated bands. Experimental and numerical study adapted to electronics thermal control. *International Journal of Heat and Fluid Flow 29*(5), 1337-1346.

Calcagni, B., F. Marsili and M. Paroncini (2005). Natural convective heat transfer in square enclosures heated from below. *Applied Thermal Engineering 25*(16), 2522-2531.

Chadwick, M., B. Webb and H. Heaton (1991). Natural convection from two-dimensional discrete heat sources in a rectangular enclosure. *International Journal of Heat and Mass Transfer 34*(7), 1679-1693.

Corcione, M. and E. Habib (2010). Buoyant heat transport in fluids across tilted square cavities discretely heated at one side. *International Journal of Thermal Sciences 49,* 797-808.

Corvaro, F. and M. Paroncini (2007). Experimental analysis of natural convection in square cavities heated from below with 2D-PIV and holographic interferometry techniques. *Experimental Thermal and Fluid Science 31*(7), 721-739.

Da Silva, A. K., S. Lorente and A. Bejan (2004). Optimal distribution of discrete heat sources on a wall with natural convection. *International Journal of Heat and Mass Transfer 47*, 203-214.

Deng, Q. H. (2008). Fluid flow and heat transfer characteristics of natural convection in square cavities due to discrete source–sink pairs. *International Journal of Heat and Mass Transfer 51*(25), 5949-5957.

Deng, Q. H. and G. F. Tang (2002). Numerical visualization of mass and heat transport for conjugate natural convection/heat conduction by streamline and heatline. *International Journal of Heat and Mass Transfer 45*(11), 2373-2385.

El Ayachi, R., A. Raji, M. Hasnaoui, M. Naimi and A. Abdelbaki (2012). Combined effects of radiation and natural convection in a square cavity submitted to two combined modes of cross gradients of temperature. *Numerical Heat Transfer, Part A. 62*, 905-931.

Flack, R. and B. Turner (1980). Heat Transfer Correlations for Use in Naturally Cooled Enclosures with High-Power Integrated Circuits. *IEEE Transactions on Components, Hybrids, and Manufacturing Technology 3*(3), 449-452.

Habib, M., S. Said and T. Ayinde (2014). Characteristics of natural convection heat transfer in an array of discrete heat sources. *Experimental Heat Transfer 27(1)*, 91-111.

Heindel, T., F. Incropera and S. Ramadhyani (1995). Conjugate natural convection from an array of discrete heat sources: part 2—a numerical parametric study. *International Journal of Heat and Fluid Flow 16*(6), 511-518.

Heindel, T., S. Ramadhyani and F. Incropera (1995). Conjugate natural convection from an array of discrete heat sources: part 1—two-and three-dimensional model validation. *International Journal of Heat and Fluid Flow 16*(6), 501-510.

Ho, C. and J. Chang (1994). A study of natural convection heat transfer in a vertical rectangular enclosure with two-dimensional discrete heating: effect of aspect ratio. *International Journal of Heat and Mass Transfer 37*(6), 917-925.

Hsu, T. H., P. T. Hsu and S. Y. Tsai (1997). Natural convection of micropolar fluids in an enclosure with heat sources. *International Journal of Heat and Mass Transfer 40*(17), 4239-4249.

Karatas, H. and T. Derbentli (2017). Natural convection in rectangular cavities with one active vertical wall. *International Journal of Heat and Mass Transfer 105*, 305-315.

Kimura, S. and A. Bejan (1983). The “heatline” visualization of convective heat transfer. *Journal of heat transfer 105*(4), 916-919.

Kuznetsov, G. V. and M. A. Sheremet (2011). Conjugate natural convection in an enclosure with a heat source of constant heat transfer rate. *International Journal of Heat and Mass Transfer 54*(1), 260-268.

Mahapatra, P. S., S. Chatterjee, A. Mukhopadhyay, N. K. Manna and K. Ghosh (2016). Proper orthogonal decomposition of thermally-induced flow structure in an enclosure with alternately active localized heat sources. *International Journal of Heat and Mass Transfer 94*, 373-379.

Mahapatra, P. S., N. K. Manna and K. Ghosh (2015). Effect of active wall location in a partially heated enclosure. *International Communications in Heat and Mass Transfer 61*, 69-77.

Mahapatra, P. S., N. K. Manna, K. Ghosh and A. Mukhopadhyay (2015). Heat transfer assessment of an alternately active bi-heater undergoing transient natural convection.

International Journal of Heat and Mass Transfer 83, 450-464.

Naffouti, T., J. Zinoubi, N. A. Che Sidik and R. B. Maad (2016). Applied thermal Lattice Boltzmann model for fluid flow of free convection in 2-D enclosure with localized two active blocks: heat transfer optimization. *Journal of Applied Fluid Mechanics 9(1)*, 419-430.

Nardini, G. and M. Paroncini (2012). Heat transfer experiment on natural convection in a square cavity with discrete sources. *Heat and Mass Transfer 48*(11), 1855-1865.

Nardini, G., M. Paroncini and R. Vitali (2016). Experimental and numerical analysis of the effect of the position of a bottom wall hot source on natural convection. *Applied Thermal Engineering 92*, 236-245.

Purusothaman, A., V. Divya, N. Nithyadevi and H. F. Oztop (2016). An analysis on free convection cooling of a 3x3 heater array in rectangular enclosure using Cu-EG-water nanofluid. *Journal of Applied Fluid Mechanics 9(6)*, 3147-3157.

Purusothaman, A., N. Nithyadevi, H. Oztop, V. Divya and K. Al Salem (2016). Three dimensional numerical analysis of natural convection cooling with an array of discrete heaters embedded in nanofluid filled enclosure. *Advanced Powder Technology 27*(1), 268-280.

Ramos, R. A. V., T. Dias and L. F. Milanez (1998). Numerical and experimental analysis of natural convection in a cavity with flush mounted heat sources on a side wall. *Proceedings of The Sixth Intersociety Conference on Thermal and Thermomechanical Phenomena in Electronic Systems, ITHERM'98*.

Tou, S. K. W. and X. F. Zhang (2003). Three-dimensional numerical simulation of natural convection in an inclined liquid-filled enclosure with an array of discrete heaters. *International Journal of Heat and Mass Transfer 46*, 127-138.

Tou, S., C. Tso and X. Zhang (1999). 3-D numerical analysis of natural convective liquid cooling of a 3× 3 heater array in rectangular enclosures. *International Journal of Heat and Mass Transfer 42*(17), 3231-3244.

Valencia, A. and R. L. Frederick (1989). Heat transfer in square cavities with partially active vertical walls. *International Journal of Heat and Mass transfer 32(8)*, 1567-1574.

Yovanovich, M. (1991). Influence of discrete heat source location on natural convection heat transfer in a vertical square enclosure. *Journal of Electronic Packaging 113*, 269.